Arabian Journal of Chemistry (2022) **15**, 104079

King Saud University

Arabian Journal of Chemistry

www.ksu.edu.sa
www.sciencedirect.com

ORIGINAL ARTICLE

Engineered polymer matrix novel biocompatible materials decorated with eucalyptus oil and zinc nitrate with superior mechanical and bone forming abilities

Mohan Prasath Mani [a], Ahmad Athif Mohd Faudzi [b,c], Shahrol Mohamaddan [d], Ahmad Fauzi Ismail [e], Rajasekar Rathanasamy [f], Manikandan Ayyar [g], Saravana Kumar Jaganathan [b,c,h,*]

[a] *School of Biomedical Engineering and Health Sciences, Faculty of Engineering, Universiti Teknologi Malaysia, Skudai 81310, Malaysia*
[b] *Centre for Artificial Intelligence and Robotics, Universiti Teknologi Malaysia, Kuala Lumpur 54100, Malaysia*
[c] *School of Electrical Engineering, Faculty of Engineering, Universiti Teknologi Malaysia, Johor Bahru 81310, Malaysia*
[d] *Department of Bioscience and Engineering, College of Systems Engineering and Science, Shibaura Institute of Technology, 337-8570 Saitama, Japan*
[e] *Advanced Membrane Technology Research Centre (AMTEC), School of Chemical and Energy Engineering, Universiti Teknologi Malaysia, Skudai 81310, Malaysia*
[f] *Department of Mechanical Engineering, Kongu Engineering College, Erode 638052, Tamil Nadu, India*
[g] *Department of Chemistry, Bharath Institute of Higher Education and Research, Bharath University, Chennai 600073, Tamil Nadu, India*
[h] *Department of Engineering, Faculty of Science and Engineering, University of Hull, Hu6 7RX, United Kingdom*

Received 9 July 2021; accepted 25 June 2022
Available online 1 July 2022

KEYWORDS

PU;
$ZnNO_3$;
EL;
Electrospinning;
Bone tissue regeneration

Abstract Electrospun scaffolds based on polymer-matrix composites have gained wide attention recently. A novel engineered biocompatible scaffold is manufactured using polyurethane (PU) loaded with eucalyptus oil (EL) and Zinc nitrate ($ZnNO_3$) using the electrospinning technique. Morphological observations revealed the reduced fibre diameter for the PU/EL and PU/EL/$ZnNO_3$ compared to PU. Contact angle studies indicated the increase in hydrophobic behaviour of the PU/EL whereas an increase in wettability for PU/EL/$ZnNO_3$ compared to PU. EL and $ZnNO_3$ presence

* Corresponding author.
E-mail addresses: jaganathaniitkgp@gmail.com, s.k.jaganathan@hull.ac.uk (S.K. Jaganathan).
Peer review under responsibility of King Saud University.

Production and hosting by Elsevier

https://doi.org/10.1016/j.arabjc.2022.104079

in the PU matrix enhanced the mechanical strength. Surface topology analysis showed a decrease in the roughness for the PU/EL and PU/EL/$ZnNO_3$ compared to the pristine PU. Both PU/EL and PU/EL/$ZnNO_3$ showed prolonged clotting time and decreased haemolytic percentage compared to the polyurethane as indicated in their anticoagulation studies. In vitro bone mineralisation testing depicted the increase in calcium deposition for the modified PU samples compared to pure polyurethane sample. Hence, PU/EL and PU/EL/$ZnNO_3$ scaffold with superior properties render full avenues for new bone generation.

1. Introduction

Bone defects may arise due to congenital (maldevelopment of bones) or acquired conditions (trauma, infection, neoplasm, or surgical resection) (Ibrahim, 2018). Orthopaedics is concerned with treating the above-mentioned bone defects and it is still a challenging task for clinicians. The commonly employable mode for repairing the bone defects was autologous bone graft and allograft. Though those methods possess better biocompatibility, it was limited because of the scarcity of donor tissues, donor site complications, disease transmission, and infections (Wang and Yeung, 2017). These limitations force the researches to explore various other alternatives for repairing the bone defects. Recently, tissue engineering has provided endless opportunities to repair and construct bones. Tissue engineering utilizes three components namely scaffolds, human cells, and biochemical clues for regeneration and repair of the damaged tissues (O'brien, 2011). Among these, the scaffolds have an important role in mimicking the function of the native extracellular matrix (ECM) and also supporting the new tissue growth by favouring the cell adhesion and proliferation (Chan and Leong, 2008; Richbourg et al., 2019). Scaffolds are produced using various manufacturing techniques and every technique utilized in one way or another tries to replicate the morphological and functional properties which are analogous to the natural ECM (Eltom et al., 2019).

Human bone is a complex material composed of type I collagen as well as inorganic materials (carbonated apatite) (Vaz et al., 2011). The scaffolds used in bone tissue replacements should be able to reproduce such environment for bone regeneration. This is partly possible through the selection of an appropriate manufacturing technique for bone scaffold fabrication. The most reputed method for scaffold production is electrospinning as it offers a large surface to volume ratio, porous structure, and good mechanical properties (Vasita and Katti, 2006; Liu et al., 2013; Kumar et al., 2018). Moreover, the plethoras of literature suggested that electrospun scaffold able to biomimic the ECM and also promote cell adhesion and proliferation for de novo tissue in-growth (Wang et al., 2013). Recently, the scaffold-based on the polymer-matrix composite is found to be widely customized in the tissue engineering application due to its tailor-made properties (Dhandayuthapani et al., 2011). Based on the literature, polyurethane is used as a base polymer due to its long-standing history in medical applications. Several recent studies suggested polyurethane-matrix composites have evolved as promising scaffolds in the skin, bone, cardiac, and other tissue engineering applications (Unnithan et al., 2012; Tetteh et al., 2014; Subramaniam et al., 2018; Kuo et al., 2014).

Two additives namely eucalyptus oil and zinc nitrate were selected in order to enhance the bone-forming abilities of polyurethane. Eucalyptus which belongs to *Myrtaceae* family is found in the subtropical and Mediterranean regions (Jerbi et al., 2017). The essential oils of eucalyptus constitute α-pinene, 1,8-cineol and pinocarveol-trans. 1,8-cineol as a major constitute accounting between 49.07 and 83.59% and the rest is α-pinene totalling nearly 1.27 to 26.35% (Sebei et al., 2015). Eucalyptus was found to be widely employed in traditional medicine owing of their properties like antibacterial, anti-inflammatory, antipyretic, disinfectant, antimalarial, antiseptic, analgesic, expectorant, and antioxidant properties. The extract of the plant was used to treat various diseases like wound healing, fungal infection, cold, chest pain, cough, influenza, skin rash, inflammation, rhinitis and sinusitis (Jerbi et al., 2017). The other constituent used in this study is zinc nitrate. Zn is an element with atomic number 30. In the human body, zinc is an essential element and performs several physiological functions which include normal growth, immune functions, synthesis of protein and DNA, and also have been linked to wound healing. Few studies have been reported electrospun scaffolds loaded with ZnO for biomedical applications. To state, Zviagin et al., 2019 developed a scaffold comprising poly(3-hydroxybutyrate) scaffolds deposited with ZnO. It was concluded that the fabricated composites with improved wettability might be suitable for the biomedical applications. In another study, Shitole et al., 2019 developed a scaffold comprising polycaprolactone scaffolds containing hydroxyapatite and ZnO. The fabricated composites displayed better antimicrobial activity and good cell biocompatibility making it ideal for bone tissue regrowth. Further, it has been reported in *vitro* studies that the occurrence of zinc influenced osteoblast cell response and inhibits bone resorption (Zhao et al., 2016; Feng et al., 2014). To our knowledge none of the studies have reported the usage and effect of EL in regenerative medicine. Reports have concluded that the incorporation of essential oils induces anti-inflammatory response however it renders hydrophobicity to the scaffold (Dhifi et al., 2016). Hydrophobic surface might be concern in bone tissue engineering which reduces the cellular responses. In order to tailor the wettability of the PU/EL scaffold, $ZnNO_3$ is introduced to the polyurethane scaffold to manipulate the scaffold wettability. Hence, the motivation of this study is to investigate the combination of EL and $ZnNO_3$ in bone tissue engineering scaffolds. Further, this study will decipher the properties and bone-forming abilities of manufactured composite scaffold along with polyurethane to understand the potential in bone tissue construction.

2. Chemicals and methods

2.1. Chemicals

Tecoflex EG-80A pellets were purchased from Lubrizol, Wickliffe, Ohio, USA. Tecoflex EG-80A is aliphatic polyether-based thermoplastic polyurethanes (TPUs). Dimethylformamide (DMF) was obtained from Sigma-Aldrich, UK. $ZnNO_3$ was bought from Sigma Aldrich, UK. Eucalyptus oil was purchased from a local vendor situated at Paradigm Mall, Johor, Malaysia. Chemicals such as phosphate-buffered saline (PBS; Biotech Grade) and sodium chloride saline (0.9% w/v) were bought from Sigma-Aldrich, Malaysia. Activated partial thromboplastin test (APTT) and prothrombin test (PT) reagents were supplied from the Thermo Fisher Scientific, Selangor, Malaysia.

2.2. Fabrication of scaffolds

Initially, 9 wt% of polyurethane solution in DMF were stirred for 12 hr. For eucalyptus oil and zinc nitrate, 4 % was used prepared by the addition of eucalyptus oil/zinc nitrate to the DMF and stirred for 1 hr. PU/EL and PU/EL/$ZnNO_3$ scaffolds were prepared by mixing EL and $ZnNO_3$ solution in PU solution at a ratio of 8:1 v/v (PU/EL) and 8:0.5:0.5 v/v (PU/EL/$ZnNO_3$) respectively and stirred for 1 hr. All solutions were stirred at room temperature using a magnetic stirrer at 500 rpm. The electrospinning technique (Progene Link Sdn Bhd, Selangor, Malaysia) was performed in room temperature and humidity (55%) with a flow rate of 0.2 mL h^{-1}, 10.5 kV voltage, and distance set at 20 cm respectively. The deposited nanofibers on the fixed mandrel were vacuum dried before characterization and testing.

2.3. Physiochemical characterization

PU, PU/EL and PU/EL/$ZnNO_3$ scaffolds were imaged using a field emission scanning electron microscope (FESEM). First, the developed nanofibers were gold coated and their morphology were viewed in Hitachi SU8020, Tokyo, Japan at an accelerating voltage of 15 kV and working distance of 6 mm. Fiber diameter was computed by importing the FESEM images inside the Image J software and minimum 30 measurements are taken at various locations to calculate the diameter. PU, PU/EL, and PU/EL/$ZnNO_3$ spectra were recorded using Nicolet iS 5, Thermo Fischer Scientific, Waltham, MA, USA equipped with ATR crystal of zinc selenium in wavelength between 600 and 4000 cm^{-1}.

The contact angles of the PU/EL and PU/EL/$ZnNO_3$ scaffolds were determined through VCA optima contact angle equipment (AST Products, Inc., Billerica, MA, USA). The medium was water and the size of droplet was 0.5 µL. The authors have used single droplet on the sample surface and three individual samples were used to measure the mean. The thermal behaviour of the electrospun PU, PU/EL, and PU/EL/$ZnNO_3$ was investigated through the thermal gravimetric analysis (TGA) unit (PerkinElmer, Waltham, MA, USA) under nitrogen atmosphere. The samples were heated in the temperature range between 30 °C and 1000 °C. The surface roughness (Ra) of PU, PU/EL, and PU/EL/$ZnNO_3$ scaffolds was measured via NanoWizard®, JPK Instruments, Berlin, Germany in taping mode with a scan area of 20 × 20 μm^2 respectively. Electrospun scaffolds were tested via uniaxial tensile machine (Gotech Testing Machines, AI-3000, Taichung City, Taiwan). Samples of size 40 X 15 mm^2 were subjected to 10 mm min^{-1} until breakage occurs.

2.4. Blood compatibility measurements

2.4.1. APTT assay

For APTT assay, a small piece of sample was incubated with platelet poor plasma (PPP) for 1 min at 37 °C. After this, it was mixed with 50 µL of rabbit brain cephaloplastin reagent and left for 3 min at 37 °C. Finally, the blood clot was activated by adding 50 µL of $CaCl_2$. The time was taken until the blood clot was formed which was given as APTT.

2.4.2. PT assay

For PT assay, a small piece of sample was incubated with PPP for 1 min at 37 °C. After, the mixture was incubated with 50 µL of NaCl–thromboplastin reagent (Factor III). The time required to blood clot was measured as PT.

2.4.3. Hemolysis assay

Initially, the freshly collected blood was diluted with normal saline. To this diluted blood, a small piece of sample was incubated for 60 min at 37 °C. After, the blood samples were centrifuged at 3000 rpm for 15 min. Finally, a supernatant solution was pipette and the absorbance was measured at 542 nm using UV–Vis spectrophotometer. The negative control used was the normal saline (no hemolysis) while the positive control was the distilled water (complete hemolysis). The hemolysis percentage was calculated from equation as reported earlier (Jaganathan and Mani, 2018).

2.5. Bioactivity test

In vitro apatite formation was used to investigate the bone-forming abilities of PU, PU/EL, and PU/EL/$ZnNO_3$. Briefly, scaffold materials were by soaked in simulated body fluid (SBF) and kept for 14 days (Srinivasan and Rajendran, 2015). The samples were taken out, washed with distilled water and dried after 14 days. Dried scaffolds were gold plated and imaged using FESEM and energy dispersive X-ay analyzer to estimate the calcium deposition. EDX was performed in point scanning with a voltage f 15 kV respectively.

2.6. Statistical analysis

All experiments were performed using three individual samples. Statistical significance was evaluated by using one-way ANOVA. The results are expressed as mean ± SD for all experiments.

3. Results and discussion

3.1. FESEM investigation

FESEM images of scaffolds were indicated in Fig. 1. The fibres formed in all three scaffolds were smooth without any beads. Further, fibres were oriented randomly in all directions as

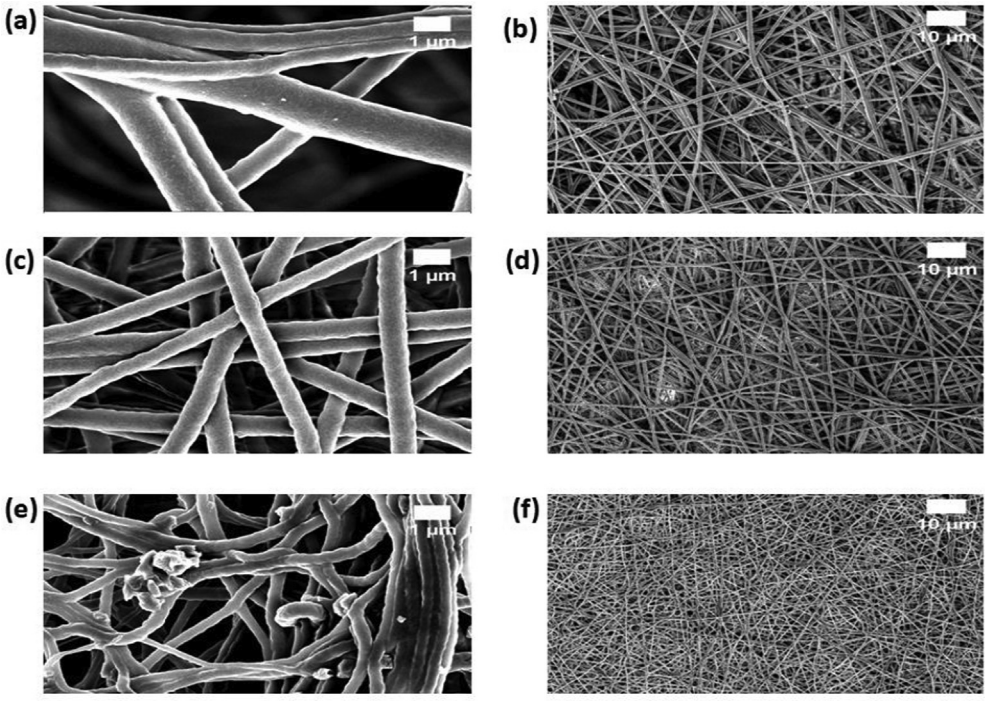

Fig. 1 FESEM images of a) PU, c) PU/EL and e) PU/EL/$ZnNO_3$ at higher magnifications and b) PU, d) PU/EL and f) PU/EL/$ZnNO_3$ at lower magnifications.

observed in Fig. 1. Image J analysis of fibre diameter distribution demonstrated the reduction of the diameter of the composites than the PU as indicated in Fig. 2. Mean diameter of the PU was estimated to be 1038 ± 147 nm, while the electrospun PU/EL and PU/EL/$ZnNO_3$ displayed diameter of 495 ± 180 nm and 340 ± 139 nm respectively. The EL oil contains several bioactive constituents such as α-pinene, 1,8-cineol and pinocarveol-trans1,8-cineol which might have altered the properties of the composite solutions resulting in the reduction of fibre diameter of PU. The fibre diameter reduction was enhanced while adding $ZnNO_3$ to the PU/EL composites. Recent works suggested that smaller fibre diameter will favour the enhanced osteoblast cell responses (Ngiam et al., 2009; Guo et al., 2017). It has been reported that cell adhesion increases with the enhanced surface area of the fiber (Ko and Yang, 2008). Since the smaller fiber diameter of the composite scaffolds renders larger surface area,it will be conducive to the cell attachment. This enhanced cell adhesion might lead to better survival and cell proliferation. The prepared PU/EL and PU/EL/$ZnNO_3$ with reduced fibre diameter will be suitable for the enhanced proliferation of osteoblast cells for de novo growth. Further, the polyurethane matrix having zinc content which was confirmed through EDX analysis. PU and PU/EL showed carbon and oxygen content whereas PU/EL/$ZnNO_3$, displayed Zn content (1.1%) in addition to that.

3.2. FTIR analysis

Fig. 3 represents the IR spectrum of the fabricated fibres from polyurethane and the novel composites. From the FTIR spectra of polyurethane, a broad peak at 3318 cm^{-1} insinuating the NH band, and peaks at 1531 cm^{-1} and 1597 cm^{-1} denotes the vibrations of NH band. The peaks at 2920 cm^{-1} and 2852 cm^{-1} were attributed to CH band, similarly 1414 cm^{-1} represented the vibrations of CH band. In continuation, peaks at 1701 cm^{-1} and 1730 cm^{-1} indicates the C = O band, and whereas peaks at 1221 cm^{-1}, 1105 cm^{-1} and 770 cm^{-1} represents C–O corresponding to alcohol (Mani et al., 2018; Chao et al., 2018). PU/EL and PU/EL/$ZnNO_3$ showed peaks were similar to pure PU scaffolds. But it was noted that the peak intensity of PU was altered (increased) with the incorporation of EL and $ZnNO_3$ and it was because of hydrogen bond formation (Unnithan et al., 2012). Moreover, CH band at 2920 cm^{-1} in PU was changed to 2941 cm^{-1} in PU/EL and 2939 cm^{-1} in PU/EL/$ZnNO_3$ respectively (Tijing et al., 2012). These changes evidenced PU matrix have EL and $ZnNO_3$.

3.3. Wettability measurements

PU scaffold displayed hydrophobic behavior with a contact angle of 105° ± 3. While adding EL, the contact angle was increased to 115° ± 1 indicating an increase in the hydrophobic nature. On adding $ZnNO_3$ to the PU/EL, wettability was reversed by decreasing the contact angle to 67° ± 1. Wettability is one of the important physicochemical parameters which play a vital role in cell adhesion and proliferation. It was revealed that the contact angle below 106° is appropriate for the proliferation of osteoblast cells (Wei et al., 2009). The contact angle of PU/EL/$ZnNO_3$ falls within the reported range suitable for facilitating the osteoblast cells growth. In a recently concluded study, a nylon-6 bone scaffold added with hydroxyapatite (HA) was manufactured. HA integration resulted in enhanced wettability of the nylon 6 and displayed enhanced apatite formation than the pure nylon-6 scaffold (Abdal-Hay et al., 2013). Hence, our PU/EL/$ZnNO_3$ signified

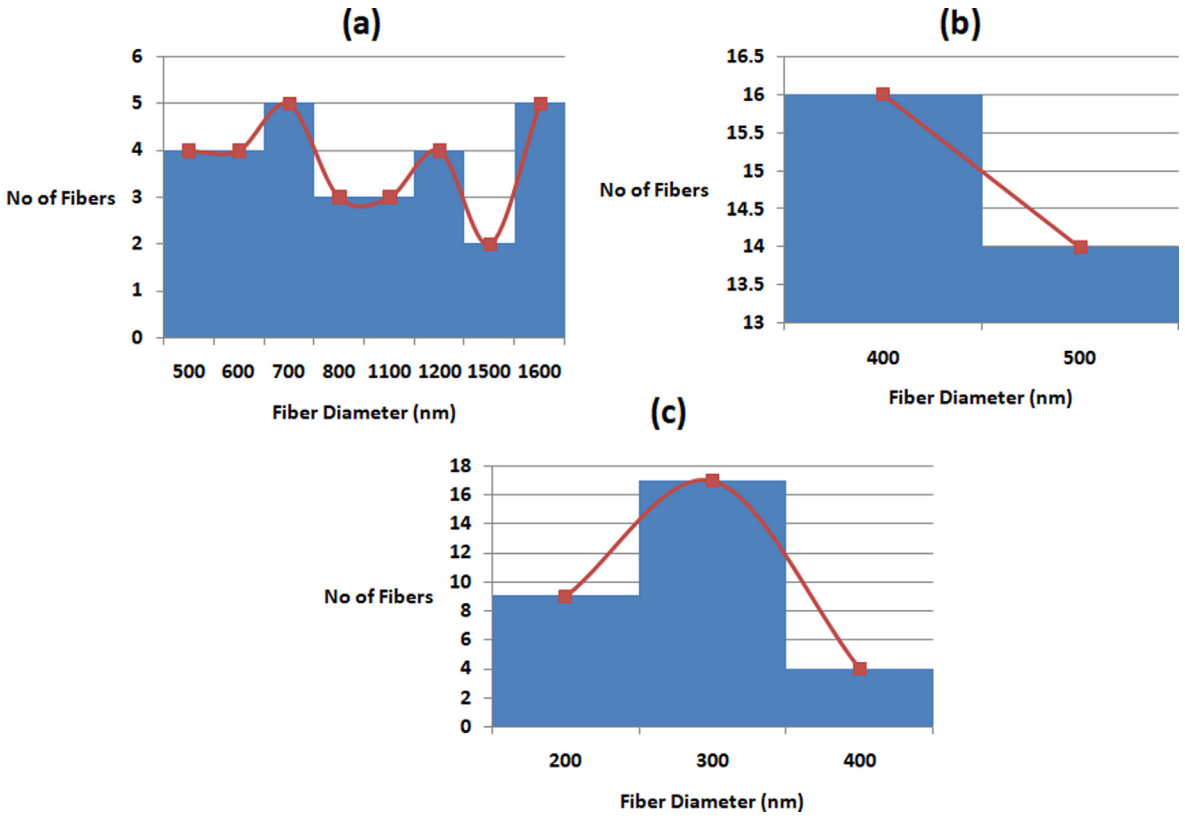

Fig. 2 Fiber distribution curves of a) PU, b) PU/EL and c) PU/EL/$ZnNO_3$.

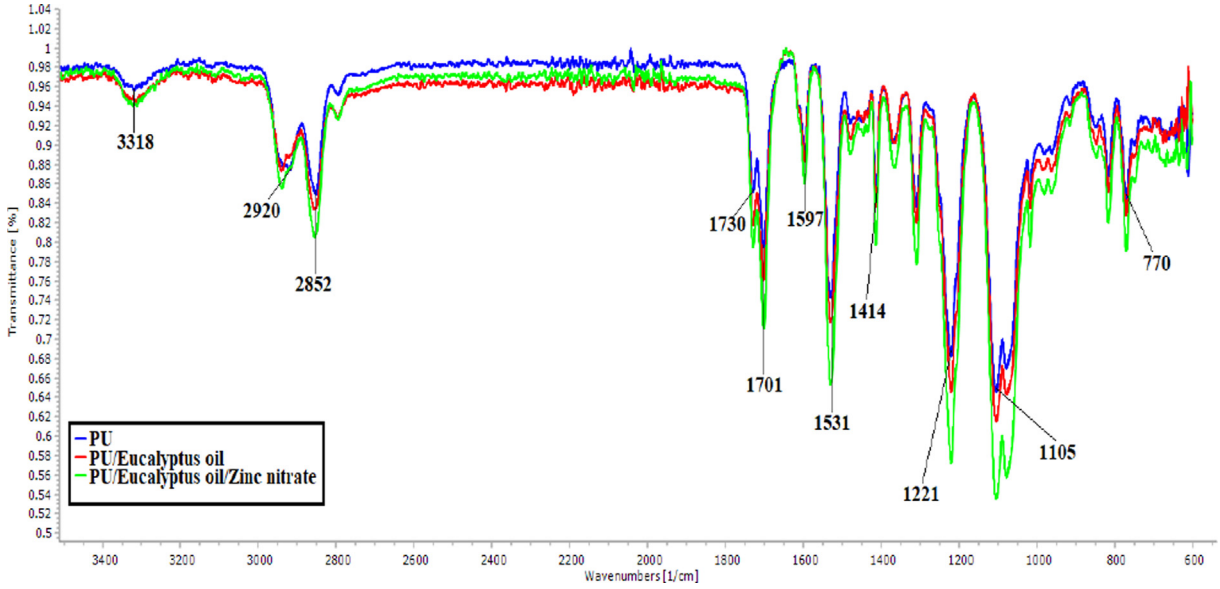

Fig. 3 FTIR images of PU, PU/EL and PU/EL/$ZnNO_3$.

improved wettability might be suitable for the enhanced apatite formation.

3.4. Thermal stability

Fig. 4 presents the TGA curves of pure fibres along with newly developed materials. From the TGA curve, it was observed the initial degradation temperature for the PU was 284 °C and for the PU/EL and PU/EL/$ZnNO_3$, the temperature was found to be 296 °C and 210 °C, respectively. Hence, the degradation temperature of PU was enhanced by adding EL whereas the addition of $ZnNO_3$ caused a reduction. Keong et al., 2017 prepared sodium alginate film with zinc nitrate added. They observed that the prepared membrane showed a first drop in

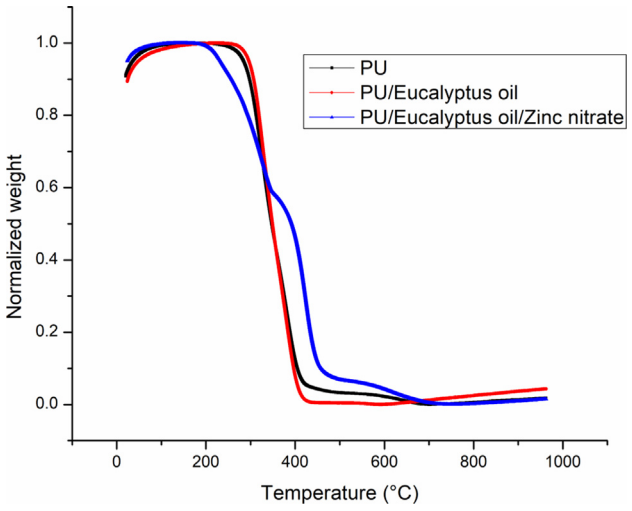

Fig. 4 TGA curve of PU, PU/EL and PU/EL/$ZnNO_3$.

weight loss at 170 °C attributed to the loosely bond water or moisture present in the sample. The reduction in the temperature of PU/EL/$ZnNO_3$ was because of the volatile water molecules present in the zinc nitrate. Moreover, the DTG curves of the PU, PU/EL, and PU/EL/$ZnNO_3$ were shown in Fig. 5. The PU showed three weight loss peaks while the fabricated composites showed two (PU/EL) and four weight loss (PU/EL/$ZnNO_3$) peaks. The first major mass loss recorded in PU nanofibers at the temperature between 208 °C and 360 °C was due to the melting of hard segments of PU. The second major weight loss at 360 °C to 512 °C may due to the decomposition of soft segments in PU. A small weight loss at 512 °C to 754 °C was due to the evaporation of volatile components. The addition of EL oil shows only three mass loss peaks at 237 °C to 364 °C, 364 °C to 516 °C and 516 °C to 781 °C respectively which are same as that of PU. However, their intensity was decreased compared to the pure PU indicating lower weight loss. The effect of incorporating $ZnNO_3$ on the thermal stability of PU/EL can be clearly noted at a temperature between 161 °C and 249 °C which might be due to the melting of volatile components present in the $ZnNO_3$. The other mass loss peaks at 249 °C to 359 °C, 359 °C to 522 °C and 522 °C to 777 °C respectively which were same as that of pure PU. However, their weight loss peak intensity was increased compared to the pure PU suggesting higher weight loss and incorporation of $ZnNO_3$ in the polyurethane matrix.

3.5. Mechanical characterization

Fig. 6 depicts the mechanical behaviour of fabricated scaffolds. PU displayed the tensile strength of 6.46 ± 0.34 MPa while the tensile strength of PU/EL and PU/EL/$ZnNO_3$ was found to be 9.41 ± 0.28 MPa and 11.26 ± 0.44 MPa, respectively. Jaganathan and Mani, 2018 observed the enhancement of the tensile strength of the polyurethane scaffold by adding copper sulphate particles that resemble our observations. They ascribed this behaviour to the reduced fibre diameter morphology of their developed composite. Shanmugavel et al., 2014 electrospun a bone scaffold and showed the tensile strength of 4 MPa was good enough for bone tissue engineering. In another study, Thomas et al., 2007 developed a scaffold based on collagen and nanohydroxyapatite (nanoHA) bone tissue engineering. The obtain tensile strength of the electrospun scaffold was reported to be 5 MPa and concluded it as a suitable candidate for bone tissue regeneration. Our tensile strength of the composite scaffolds was better than the highlighted value suggesting their potential application for bone tissue engineering. Our tensile strength was better than those reported values making PU/EL and PU/EL/$ZnNO_3$ as appropriate candidates for bone tissue engineering.

3.6. Surface roughness measurements

Fig. 7 presents surface images of PU/EL and PU/EL/$ZnNO_3$. PU showed an average Ra of 854 ± 32 nm, while the Ra for the PU/EL and PU/EL/$ZnNO_3$ was 634 ± 278 nm and 437 ± 144 nm respectively. It depicted the smoother surface for PU/EL and PU/EL/$ZnNO_3$. The active constituents of EL and the interaction of the components added might have caused the smooth surfaces. Kim et al., 2016 studied the effect of the fibre diameter on the surface roughness in electrospun poly (e–caprolactone) (PCL) fibers. It have been reported that the scaffold with a smaller diameter showed a decreased in roughness value compared to the larger fiber diameter. Hence,

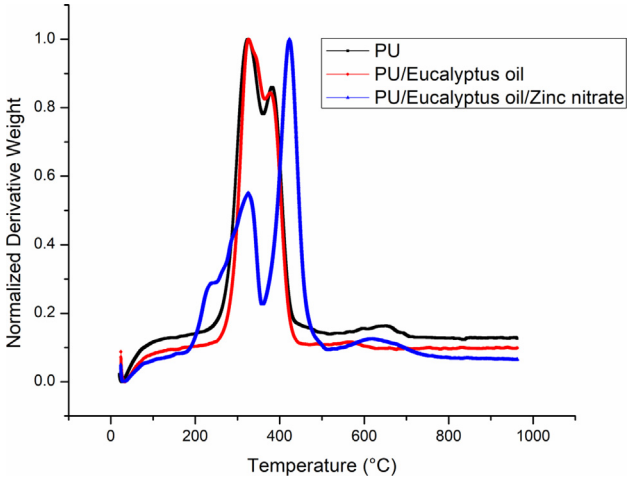

Fig. 5 DTG curve of PU, PU/EL and PU/EL/$ZnNO_3$.

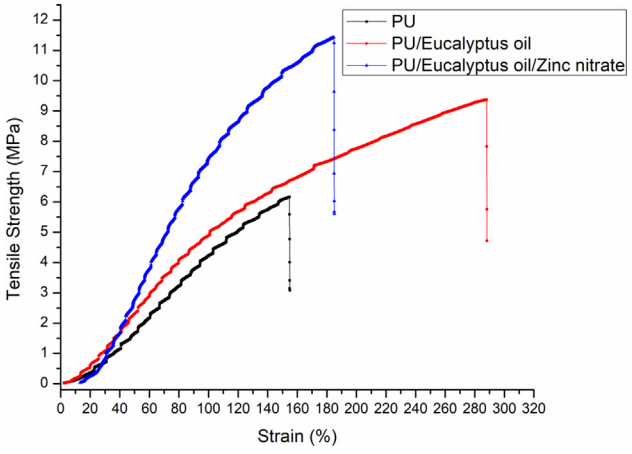

Fig. 6 Tensile curves of PU, PU/EL and PU/EL/$ZnNO_3$.

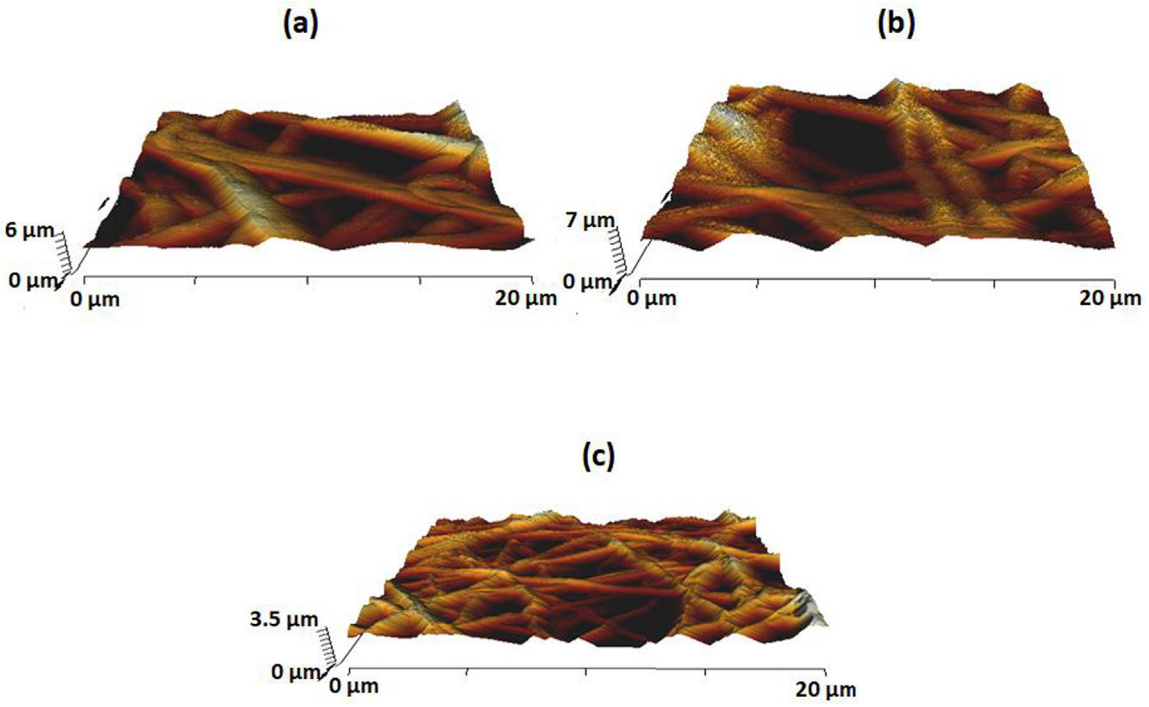

Fig. 7 AFM images of a) PU, b) PU/EL and c) PU/EL/$ZnNO_3$.

our composite scaffold with smaller diameter than the pure PU might resulted in the decrease in surface roughness value.

3.7. Blood compatibility measurements

Coagulation analysis such as APTT, PT, and haemolysis was done to determine the blood compatible behaviour and are displayed in Fig. 8. Activated partial thromboplastin time (APTT) for the PU fibres were measured to be 176 ± 2 s and for the PU/EL and PU/EL/$ZnNO_3$, it was estimated to be 198 ± 1 s and 193 ± 4 s respectively as shown in Fig. 8a. Similarly, PT assay results for the PU membrane was calculated to be 94 ± 2 s and for the PU/EL and PU/EL/$ZnNO_3$ it was estimated to be 108 ± 1 sand 106 ± 1 s respectively as shown in Fig. 8b. The delay in the clotting time is attributed to EL and $ZnNO_3$ in the PU matrix. The prepared nanocomposites exhibited less hemolytic percentage of 1.71% (PU/EL) and 1.77% (PU/EL/$ZnNO_3$) compared to the pristine PU where it was 2.83% as shown in Fig. 8c. The values of composites were below 2% and hence they are classified as non-hemolytic material as per ASTMF756-00 (Mani et al., 2018; Chao et al., 2018). PU/EL and PU/EL/$ZnNO_3$ were compatible with the blood than the PU. The PU/EL displayed higher blood clotting time than PU/EL/$ZnNO_3$ which

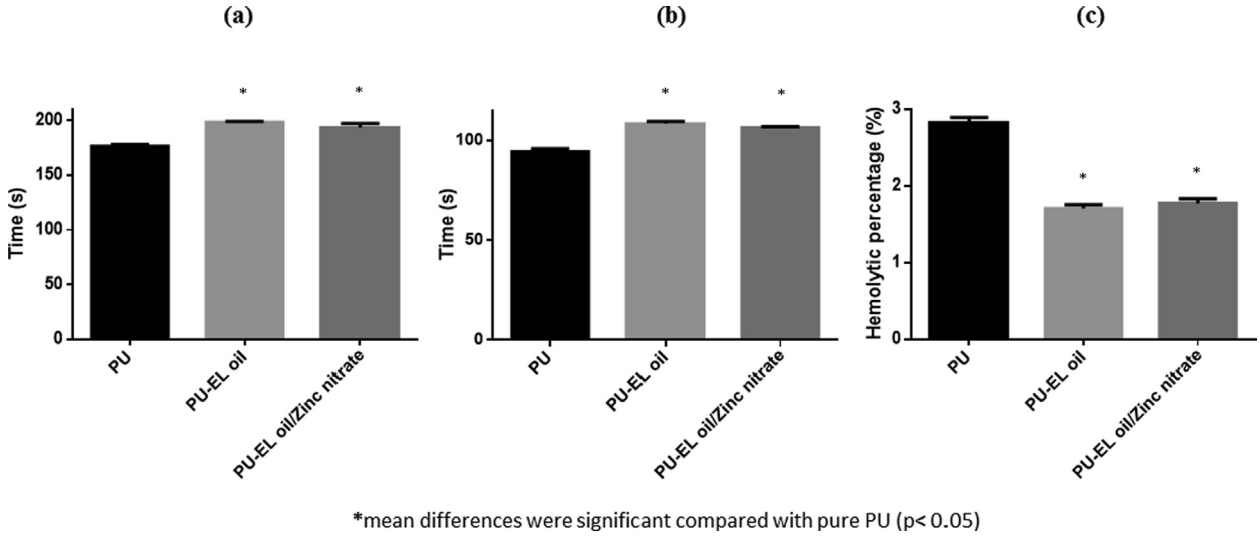

Fig. 8 a) APTT, b) PT and c) Hemolytic index of PU, PU/EL and PU/EL/$ZnNO_3$.

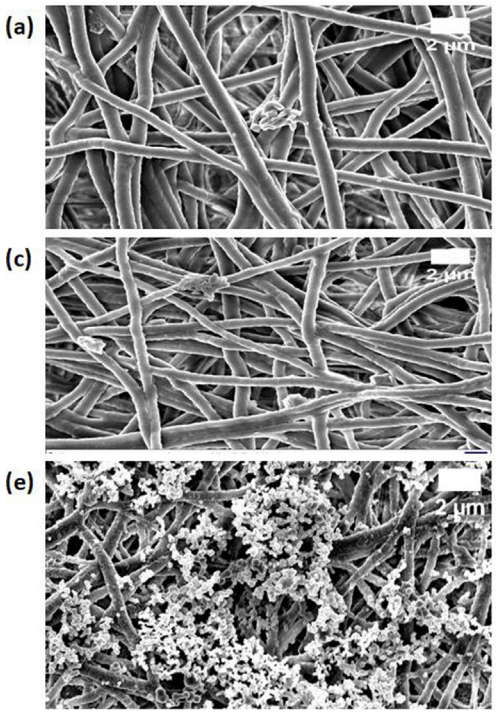

(b)

Element	Wt (%)	σ
C	74.4	0.6
O	22.1	0.5
Ca	2.4	0.3
P	1	0.3

(d)

Element	Wt (%)	σ
C	67.7	0.9
O	24.2	0.8
Ca	6.7	0.7
P	1.4	0.4

(f)

Element	Wt (%)	σ
C	48.7	0.8
O	32.7	0.7
Ca	13.1	0.7
P	5.4	0.4

Fig. 9 FESEM images of bone mineralization in electrospun membranes a) PU, c) PU/EL and e) PU/EL/ZnNO3 and their corresponding EDX analysis b) PU, d) PU/EL and f) PU/EL/ZnNO3.

was due to their hydrophobic surface. It was postulated that the surface of hydrophobic would adhere to plasma proteins irreversibly resulting in prolonging the blood compatibility behaviour (Sandejas, 2016). The slight decrease in the blood clotting time of PU/EL/$ZnNO_3$ than the PU/EL which might due to the change in the polarity regions (Szycher, 1991). Literature has suggested that blood compatibility behaviour was also affected by various physicochemical properties (Huang et al., 2003). Literature has been reported that the scaffold showing hydrophobic behaviour and smaller fibre diameter might increase the blood clotting time (Li et al., 2019). The composites displayed smaller fibre diameter (PU/EL and PU/EL/$ZnNO_3$) and hydrophobic nature (PU/EL) which would have influenced the blood compatibility behaviour.

3.8. Bone mineralisation testing

Bone forming abilities of PU/EL and PU/EL/$ZnNO_3$ scaffold in comparison with PU were done to promote it for bone tissue engineering as shown in Fig. 9. Morphology analysis of FESEM images confirmed the significant precipitation of deposits visible on PU/EL/$ZnNO_3$ scaffolds. Further, an increased percentage of calcium deposition in the PU/EL/$ZnNO_3$ samples clearly signifies their potential application in bone tissue engineering. Hence, the addition of EL and $ZnNO_3$ might accelerated the calcium deposition of the pure PU scaffolds. Heydari et al., 2017 designed an electrospun polycaprolactone loaded with octacalcium phosphate and observed increased calcium deposition than the pure PCL bone scaffolds as similar to our reported findings. Hence, the fabricated composites with enhanced calcium deposition will be conducive for bone tissue engineering.

4. Conclusion

PU/EL and PU/EL/$ZnNO_3$ displayed significant advantage of offering superior physicochemical properties like beadless fibre morphology, wettability, surface roughness, and thermal stability. These properties positively influenced its blood compatibility, mechanical strength, and bone-forming ability. Since PU fibres are also beadles, it is worth investigating different polyurethane and additives composition in confirming the role of the fibre diameter and roughness. Hence, the newly developed PU/EL and PU/EL/$ZnNO_3$ displayed desirable physicochemical and bone-forming properties that can be potentially utilized for bone tissue engineering scaffolds. The bone mineralisation test concluded the beneficial effect of the fabricated scaffolds. However, it would be interesting to test the osteoblast cell proliferation on this scaffold in order to promote this scaffold as an emerging candidate in bone tissue engineering.

Declaration of Competing Interest

The authors declare that they have no known competing financial interests or personal relationships that could have appeared to influence the work reported in this paper.

Acknowledgement

The authors would like to acknowledge the sponsor provided by Ministry of Higher Education Malaysia (MOHE) through support under Fundamental Research Grant Scheme (FRGS/1/2019/TK04/UTM/02/41). The authors also would like to express appreciation to Universiti Teknologi Malaysia which makes this research viable and effective.

References

Abdal-Hay, A., Pant, H.R., Lim, J.K., 2013. Super-hydrophilic electrospun nylon-6/hydroxyapatite membrane for bone tissue engineering. Eur. Polym. J. 49 (6), 1314–1321.

Chan, B.P., Leong, K.W., 2008. Scaffolding in tissue engineering: general approaches and tissue-specific considerations. Eur. Spine. J. 17 (4), 467–479.

Chao, C.Y., Mani, M.P., Jaganathan, S.K., 2018. Engineering electrospun multicomponent polyurethane scaffolding platform comprising grapeseed oil and honey/propolis for bone tissue regeneration. PLOS. One 13 (10), 1–17.

Dhandayuthapani, B., Yoshida, Y., Maekawa, T., Kumar, D.S., 2011. Polymeric scaffolds in tissue engineering application: a review. Int. J. Polym. Sci. 2011, 1–19.

Dhifi, W., Bellili, S., Jazi, S., Bahloul, N., Mnif, W., 2016. Essential oils' chemical characterization and investigation of some biological activities: A critical review. Medi. 3 (4), 25.

Eltom, A., Zhong, G., Muhammad, A., 2019. Scaffold techniques and designs in tissue engineering functions and purposes: a review. Adv. Mater. Sci. Eng. 2019, 1–13.

Feng, P., Wei, P., Shuai, C., Peng, S., 2014. Characterization of mechanical and biological properties of 3-D scaffolds reinforced with zinc oxide for bone tissue engineering. PLOS. One. 9 (1), 1–13.

Guo, Z., Ma, M., Huang, X., Li, H., Zhou, C., 2017. Effect of Fibre Diameter on Proliferation and Differentiation of MC3T3-E1 Pre-Osteoblasts. J. Biomater. Tissue. Eng. 7, 162–169.

Heydari, Z., Mohebbi-Kalhori, D., Afarani, M.S., 2017. Engineered electrospun polycaprolactone (PCL)/octacalcium phosphate (OCP) scaffold for bone tissue engineering. Mater. Sci. Eng: C. 81, 127–132.

Huang, N., Yang, P., Leng, Y.X., Chen, J.Y., Sun, H., Wang, J., Wang, G.J., Ding, P.D., Xi, T.F., Leng, Y., 2003. Hemocompatibility of titanium oxide films. Biomater. 24, 2177–2187.

Ibrahim, A., 2018. 3D bioprinting bone. In: 3D Bioprint Reconstruct Surg. 245-275.

Jaganathan, S.K., Mani, M.P., 2018. Electrospun polyurethane nanofibrous composite impregnated with metallic copper for wound-healing application. 3 Biotech. 8 (8), 327.

Jerbi, A., Derbali, A., Elfeki, A., Kammoun, M., 2017. Essential oil composition and biological activities of Eucalyptus globulus leaves extracts from Tunisia. J. Essent. Oil. Bear. Plants. 20 (2), 438–448.

Kim, H.H., Kim, M.J., Ryu, S.J., Ki, C.S., Park, Y.H., 2016. Effect of fiber diameter on surface morphology, mechanical property, and cell behavior of electrospun poly (ε-caprolactone) mat. Fiber. Polym. 17, 1033–1042.

Ko, F.K., Yang, H., 2008. Functional nanofibre: enabling material for the next generations smart textiles. J. Fiber. Bioeng. Informat. 1 (2), 81–92.

Keong, C.C., Vivek, Y.S., Salamatinia, B., Horri, B.A., 2017. Green synthesis of ZnO nanoparticles by an alginate mediated ion-exchange process and a case study for photocatalysis of methylene blue dye. In. J. Phys: Conf. Series. 829, (1) 012014.

Kumar, V., Naqvi, S., Gopinath, P., 2018. Applications of Nanofibres in Tissue Engineering. In. Appl. Nanomater., 179–203

Kuo, Y.C., Hung, S.C., Hsu, S.H., 2014. The effect of elastic biodegradable polyurethane electrospunnanofibres on the differentiation of mesenchymal stem cells. Colloids. Surf. B: Biointerface. 122, 414–422.

Li, G., Li, P., Chen, Q., Mani, M.P., Jaganathan, S.K., 2019. Enhanced mechanical., thermal and biocompatible nature of dual component electrospun nanocomposite for bone tissue engineering. PeerJ. 7, e6986.

Liu, H., Ding, X., Zhou, G., Li, P., Wei, X., Fan, Y., 2013. Electrospinning of nanofibres for tissue engineering applications. J. Nanomater. 2013, 1–11.

Mani, M.P., Jaganathan, S.K., Khudzari, A.Z., Rathanasamy, R., Prabhakaran, P., 2018. Single-stage electrospun innovative combination of polyurethane and neem oil: synthesis, characterization and appraisal of blood compatibility. J. Bioact. Comp. Polym. 33 (6), 573–584.

Ngiam, M., Liao, S., Patil, A.J., Cheng, Z., Chan, C.K., Ramakrishna, S., 2009. The fabrication of nano-hydroxyapatite on PLGA and PLGA/collagen nanofibrous composite scaffolds and their effects in osteoblastic behavior for bone tissue engineering. Bone 45 (1), 4–16.

O'brien, F.J., 2011. Biomaterials & scaffolds for tissue engineering. Mater. Today 14 (3), 88–95.

Richbourg, N.R., Peppas, N.A., Sikavitsas, V.I., 2019. Tuning the biomimetic behavior of scaffolds for regenerative medicine through surface modifications. J. Tissue. Eng. Regen. Med. 13 (8), 1275–1293.

Sandejas, D., 2016. Surface Modification of a Blood Contacting Polydimethylsiloxane Microfluidic Oxygenator, Doctoral dissertation.

Sebei, K., Sakouhi, F., Herchi, W., Khouja, M.L., Boukhchina, S., 2015. Chemical composition and antibacterial activities of seven Eucalyptus species essential oils leaves. Biol. Res. 48 (1), 7.

Shitole, A.A., Raut, P.W., Sharma, N., Giram, P., Khandwekar, A.P., Garnaik, B., 2019. Electrospun polycaprolactone/hydroxyapatite/ZnO nanofibers as potential biomaterials for bone tissue regeneration. J. Mater. Sci: Mater. Med. 30 (5), 1–7.

Shanmugavel, S., Reddy, V.J., Ramakrishna, S., Lakshmi, B.S., Dev, V.G., 2014. Precipitation of hydroxyapatite on electrospunpolycaprolactone/aloe vera/silk fibroin nanofibrous scaffolds for bone tissue engineering. J. Biomater. Appl. 29 (1), 46–58.

Srinivasan, A., Rajendran, N., 2015. Surface characteristics, corrosion resistance and MG63 osteoblast-like cells attachment behaviour of nano SiO 2–ZrO 2 coated 316L stainless steel. RSC. Adv. 5 (33), 26007–26016.

Subramaniam, R., Mani, M.P., Jaganathan, S.K., 2018. Fabrication and testing of electrospun polyurethane blended with chitosan nanoparticles for vascular graft applications. Cardiovas. Eng. Technol. 9 (3), 503–513.

Szycher, M., 1991. High performance biomaterials: a complete guide to medical and pharmceutical applications. CRC Press, Boca Raton.

Tetteh, G., Khan, A.S., Delaine-Smith, R.M., Reilly, G.C., Rehman, I. U., 2014. Electrospun polyurethane/hydroxyapatite bioactive Scaffolds for bone tissue engineering: The role of solvent and hydroxyapatite particles. J. Mech. Behavior. Biomed. Mater. 39, 95–110.

Thomas, V., Dean, D.R., Jose, M.V., Mathew, B., Chowdhury, S., Vohra, Y.K., 2007. Nanostructured biocomposite scaffolds based on collagen coelectrospun with nanohydroxyapatite. Biomacromol. 8 (2), 631–637.

Tijing, L.D., Ruelo, M.T.G., Amarjargal, A., Pant, H.R., Park, C.H., Kim, D.W., Kim, C.S., 2012. Antibacterial and superhydrophilic electrospun polyurethane nanocomposite fibres containing tourmaline nanoparticles. Chem. Eng. J. 197, 41–48.

Unnithan, A.R., Pichiah, P.T., Gnanasekaran, G., Seenivasan, K., Barakat, N.A., Cha, Y.S., Jung, C.H., Shanmugam, A., Kim, H.Y., 2012. Emu oil-based electrospun nanofibrous scaffolds for wound skin tissue engineering. Colloids. Surf A: Physicochem. Eng. Asp. 415, 454–460.

Vasita, R., Katti, D.S., 2006. Nanofibres and their applications in tissue engineering. Int. J. Nanomed. 1 (1), 15.

Vaz, M.F., Canhão, H., Fonseca, J.E., 2011. Bone: a composite natural material. Adv. Comp. Mater—Analy. Natural. Man-Made Mater. 2011, 195–228.

Wang, W., Yeung, K.W., 2017. Bone grafts and biomaterials substitutes for bone defect repair: A review. Bioact. Mater. 2 (4), 224–247.

Wang, X., Ding, B., Li, B., 2013. Biomimetic electrospun nanofibrous structures for tissue engineering. Mater. Today. 16 (6), 229–241.

Wei, J., Igarashi, T., Okumori, N., Igarashi, T., Maetani, T., Liu, B., Yoshinari, M., 2009. Influence of surface wettability on competitive protein adsorption and initial attachment of osteoblasts. Biomed. Mater. 4, (4) 045002.

Zhao, L., Zhang, Z., Song, Y., Liu, S., Qi, Y., Wang, X., Wang, Q., Cui, C., 2016. Mechanical properties and in vitro biodegradation of newly developed porous Zn scaffolds for biomedical applications. Mater. Design. 108, 136–144.

Zviagin, A.S., Chernozem, R.V., Surmeneva, M.A., Pyeon, M., Frank, M., Ludwig, T., Tutacz, P., Ivanov, Y.F., Mathur, S., Surmenev, R.A., 2019. Enhanced piezoelectric response of hybrid biodegradable 3D poly (3-hydroxybutyrate) scaffolds coated with hydrothermally deposited ZnO for biomedical applications. Eur. Polym. J. 117, 272–279.